# Pauli blocking dynamics in optically excited quantum dots: A picosecond excitation-correlation spectroscopic study

Richarj Mondal,[1] Bhavtosh Bansal,[1,*] Arjun Mandal,[2] Subhananda Chakrabarti,[2] and Bipul Pal[1,†]
[1]*Indian Institute of Science Education & Research, Kolkata, Mohanpur, Nadia 741252, West Bengal, India*
[2]*Department of Electrical Engineering, Indian Institute of Technology–Bombay, Mumbai 400076, India*
(Received 26 November 2012; revised manuscript received 11 February 2013; published 25 March 2013)

State-filling dynamics in self-assembled InAs/GaAs quantum dots (QDs) is studied through their steady-state photoluminescence (PL) using a variant of picosecond excitation-correlation (EC) spectroscopy. Steady-state PL showed an interesting transition from bimolecular recombination at low-excitation fluence to excitonic recombination at higher fluence. As for the EC signal, while the ground-state response is always snubbed when the two excitation pulses are temporally nearly coincident, the excited-state response can either be enhanced or reduced, depending on the excitation fluence. The time evolution of this response is studied for the first three levels in a QD ensemble. A minimal theoretical model, which combines carrier loss kinetics with the principle of detailed balance and the Pauli exclusion principle, quantitatively reproduces the observations.

DOI: 10.1103/PhysRevB.87.115317 PACS number(s): 78.67.Hc, 73.21.La, 78.47.jd, 78.47.da

Pauli's exclusion principle is the cornerstone in the physics of the many fermions in the finite systems. The phenomenon of Pauli blocking, i.e., the physical manifestation of the exclusion principle, at the most fundamental level, is of course responsible for the stability of matter. It is also important in the study of specific physical processes of interest in fields ranging from nuclear physics[1] to cold atomic gases[2] to semiconductor devices.[3]

Semiconductor quantum dots (QDs), the so-called artificial atoms,[4] are suitable for the study of the Pauli blocking phenomenon in mesoscopic systems. Due to the sharp and discrete structure of the density of states and the fact that the number of carriers in a QD can be controllably manipulated through electrical and/or optical means,[4] QDs allow for the realization of many atomic physics concepts within the condensed matter physics domain of more accessible length and energy scales. Various properties of the discrete energy levels in QDs have been investigated over the past two decades through a variety of transport and optical experiments.[4–16] The first few discrete energy levels are commonly seen in photoluminescence (PL) experiments under high optical excitation.[8–10,14] The radiative recombination of carriers from the higher-energy states can be resolved in the PL spectra at high-excitation fluence as the lower-energy levels get filled, giving evidence of the Pauli exclusion principle at work.[8] The Coulomb blockade observed in transport through single QDs is another such example.[17]

In this paper we demonstrate the Pauli blocking phenomenon more directly and quantitatively through the time-resolved dynamics of carrier redistribution between the discrete energy states in the self-assembled InAs/GaAs QDs. The dynamics of the PL decay from the ground and the excited states in QDs has been investigated by many groups using time-resolved PL measurements.[7–12] Such studies gave valuable information on the carrier capture and intersublevel relaxation, e.g., via the carrier-carrier and carrier-phonon interactions and the Auger processes in QDs.[18] The fermionic exclusion and the state-filling effects in QDs have also been investigated.[8,10] However, state filling and saturation are essentially nonlinear phenomena. Conventional time-resolved PL measurements are unable to give explicit insight into these effects. Various types of two-beam time-resolved differential and/or correlation spectroscopies are better suited for this.[12–16]

We have developed a variant of picosecond excitation-correlation (EC) spectroscopy[14,19,20] that specifically probes the time-resolved dynamics of the nonlinear PL signal. The schematic diagram of our experimental setup is shown in Fig. 1. Here a train of pulses from a mode-locked Ti:sapphire laser, giving pulses of ∼100-fs duration at 80-MHz repetition rate, were split into two beams of equal fluence. The arrival of the pulses on the sample from one of the two beams was controllably delayed with respect to the corresponding pulses from the other beam by up to ±500 ps, with ∼300-fs resolution, by using a moving-stage retroreflector arrangement. The two beams were cofocused to the same spot of diameter ∼50 $\mu$m on the sample. The emitted PL from the sample was dispersed in a 30-cm-focal-length grating monochromator and detected by a liquid-$N_2$-cooled InGaAs linear array detector with ∼0.3-meV spectral resolution.

Note that (i) the number of photons incident on the sample is constant over one cycle (12.5 ns) of the laser pulse regardless of the set delay $\tau$ between the two excitation pulses, (ii) the array detector measures the spectrally resolved but time-integrated (over many cycles of laser pulses) PL signal emanating from the sample at a given delay, and (iii) the measurement is repeated as a function of delay to get the time evolution of the signal. We define the EC signal in our experiments as the numerically calculated difference between the PL signal at any finite delay $\tau$ and that at $\tau = 0$, viz.,

$$EC(\tau,\hbar\omega) \equiv PL_{12}(\tau,\hbar\omega) - PL_{12}(\tau = 0,\hbar\omega). \qquad (1)$$

Here $PL_{12}(\tau,\hbar\omega)$ is the steady-state PL signal measured at an energy $\hbar\omega$ with both beams incident on the sample with a delay $\tau$ between them. If there were no nonlinearity in the PL spectrum, the EC signal as a function of delay would be zero. A nonzero EC signal is a signature of PL nonlinearity.

Our experimental method and definition of the EC signal [Eq. (1)] are different from those conventionally used.[14,19,20] The EC signal is usually defined in the literature[19] as

$$\mathcal{EC}(\tau,\hbar\omega) \equiv PL_{12}(\tau,\hbar\omega) - 2PL_1(\hbar\omega). \qquad (2)$$

 

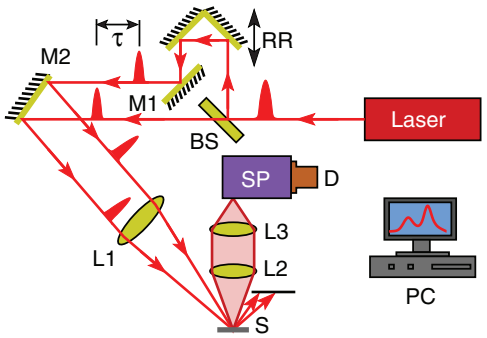


FIG. 1. (Color online) Schematic of our EC setup: BS, beam splitter; RR, retroreflector; M1 and M2, mirrors; L1, L2, and L3, lenses; S, sample; SP, spectrometer; and D, array detector.

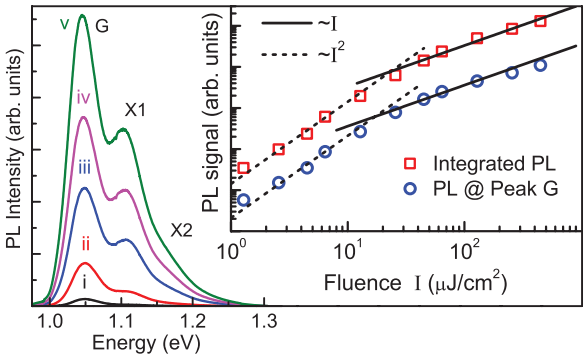


FIG. 2. (Color online) Photoluminescence spectra at different excitation fluences $I$ showing multiple peaks at higher fluence. Curves i–v correspond to $I = 13, 45, 128, 256$, and $448\ \mu\text{J/cm}^2$, respectively. Three clearly visible peaks are assigned, respectively, to the ground (G), the first excited (X1), and the second excited (X2) excitonic states. The inset shows the excitation fluence dependence of the spectrally integrated (between 0.95 and 1.3 eV) PL (□) and the PL intensity at the peak G (◯) on a log-log plot. Data are fitted with a quadratic (linear) $I$ dependence in the low- (high-) excitation fluence regime. While linearity continues for the integrated PL up to the highest fluence, the PL signal at the peak G begins to show sublinearity at high fluence.

Here $PL_1(\hbar\omega)$ is the steady-state PL measured when the sample is excited by only one of the two laser beams. While both definitions [Eqs. (1) and (2)] contain information about the dynamics of the nonlinear PL signal, the EC signal defined through Eq. (1) is much simpler to interpret. It just measures whether the time-integrated PL signal from a particular energy state under two-beam excitation decreases or increases (in reference to the signal at $\tau = 0$) as a function of delay, when the system would have lost, through various recombination channels, some carriers among those excited by the first pulse. This provides a quantitative measure of the nonlinear effects associated with the redistribution and recombination of carriers. The simplicity in the interpretation of the numerically calculated difference makes the definition of the EC signal through Eq. (1) particularly attractive because the correct interpretation of the EC signal has been a major deterrent in the wider use of this powerful technique.[21] Our experiments also take advantages of using a modern array detector instead of a point detector such as a photomultiplier tube, used in conventional EC measurements described, e.g., in Ref. 19.

The QD sample used here had two layers, each 2.7 monolayers thick, of self-assembled InAs/GaAs QDs grown via the Stranski-Krastanow mode using the solid source molecular beam epitaxy (Riber SYS14020 Epineat III-V) technique. Each layer of the QDs was capped by a 50-nm-thick intrinsic GaAs layer. Growth ended with 2.7-monolayer-thick InAs surface QDs. An atomic force micrograph on the surface QDs showed that the QDs have a base diameter of ∼60 nm, height of ∼7 nm, and dot density of $\sim 1.7 \times 10^{10}\ \text{cm}^{-2}$. We measured the time-integrated PL spectra from the QD ensemble at different excitation fluences $I$ at room temperature. The excitation wavelength (energy) was centered at 790 nm (1.57 eV), for which carriers are mostly excited in the GaAs matrix. We estimated an electron-hole pair sheet density of $\sim 1.7 \times 10^{12}\ \text{cm}^{-2}$ for an excitation fluence $I = 1\ \mu\text{J/cm}^2$, assuming an absorption coefficient[22] of $10^4\ \text{cm}^{-1}$ and a reflectance[23] of 0.3 for a GaAs layer of nominal thickness 1 $\mu$m. A fraction of these carriers is captured by the InAs QDs within a few picoseconds.[11,13,15] Later, some of them radiatively recombine to give PL in ∼1-ns time scale.[9]

The PL spectra measured at $T = 300$ K for different excitation fluences are shown in Fig. 2. Only a single peak due to the ground-state PL is seen at low fluence. With increasing excitation fluence additional peaks due to the excited states progressively become visible. This is of course the well-studied signature of the Pauli blocking in QDs.[8] We assign the three peaks appearing at about 1.05, 1.10, and 1.15 eV to the ground (G), the first excited (X1), and the second excited (X2) bright excitonic states, respectively.

It is interesting to note that the excitation fluence dependence of the spectrally integrated PL gives insight into the capture of carriers by the QDs. The variation of the spectrally integrated PL signal (□) and the PL intensity at the peak G (◯) with the excitation fluence is shown on a log-log plot in Fig. 2 (inset). The transition from the quadratic dependence on the excitation fluence $I$ below $I_{th} \approx 20\ \mu\text{J/cm}^2$ to a linear dependence above $I_{th}$ marks the presence of two physically distinct regimes. Though a quantitative estimate of the number of electrons and holes captured by a QD at a given fluence is difficult due to uncertainties in several parameters, one can quite generally argue that below $I_{th}$ there is less than one electron (or hole) captured per QD, on average. Then, if there is one electron in a QD, it is not necessary that a hole will also be present in the same QD. Since the capture of electrons and holes by QDs are independent events,[12] the rate of radiative recombination will depend on the product of the electron and hole densities, $R \sim np$. Since the electron (hole) density $n$ ($p$) is linear in excitation fluence $I$, the PL intensity will increase as $\sim I^2$. This is similar to band-to-band bimolecular recombination[24] observed in intrinsic bulk semiconductors. However, above $I_{th}$, a hole (electron) preferentially goes to a QD where an electron (hole) is already present due to the Coulomb-biased diffusion of the photoexcited carriers. This marks the onset of an exciton-like monomolecular recombination regime. The radiative recombination rate in this case will be proportional to $n$ (or $p$) and PL intensity will increase as $\sim I$.

A quadratic dependence of the PL on the excitation fluence due to biexcitonic recombination at high excitation

has been reported in the literature for low-temperature PL measurements.[25] We do not observe any superlinear fluence dependence of the PL under high-excitation fluence in our room-temperature experiments. Biexcitons are unstable at high temperature in our experiment most likely because the biexciton binding energy is very small, ∼4 meV.[26] It is also much smaller than the energy difference between (and linewidth of) the QD states. The linear dependence on excitation fluence of the spectrally integrated PL in our measurements continues up to the highest fluence ($I = 448\ \mu J/cm^2$) used. This suggests that for the *nonresonant* excitation used here, the carrier generation process does not saturate up to this fluence, unlike the case of resonant excitation of excitons.[27] Our EC measurements are confined in this linear regime. Thus any nonlinear PL signal that may be observed in our EC experiments would mostly come from the carrier redistribution and recombination process among the QD states. We exclude interdot carrier transfer from our discussion because it is not expected to contribute significantly to the carrier redistribution process at the moderate dot density of $\sim 1.7 \times 10^{10}\ cm^{-2}$ in our sample.

Figures 3(a) and 3(b) show the spectrally resolved, normalized EC signal at $\tau = 400$ ps for the QDs at $T = 300$ K for $I = 2 \times 38$ and $2 \times 192\ \mu J/cm^2$, respectively. The corresponding normalized PL spectra are also plotted on the respective graphs for a direct comparison of the PL and the EC spectra. Three peaks, associated with the G, X1, and X2 states, can be resolved in the PL spectra. The EC spectra show a positive correlation [as defined by Eq. (1)] for the G state. This means that the PL emission at nonzero delay is larger than that at zero delay ($\tau = 0$) for this state. This indicates that at $\tau = 0$, when both pulses are temporally coincident on the sample, the G state gets saturated by carriers. The sign of the EC signal for the X1 state changes from negative to positive between Figs. 3(a) and 3(b), indicating that at higher excitation fluence, this state also becomes saturated with carriers.[14] We observed no detectable lattice heating by photoexcitation up to the highest fluence used in our room-temperature experiments. This was ascertained by the fact that the PL peak energies were found to be independent of the excitation fluence; lattice heating

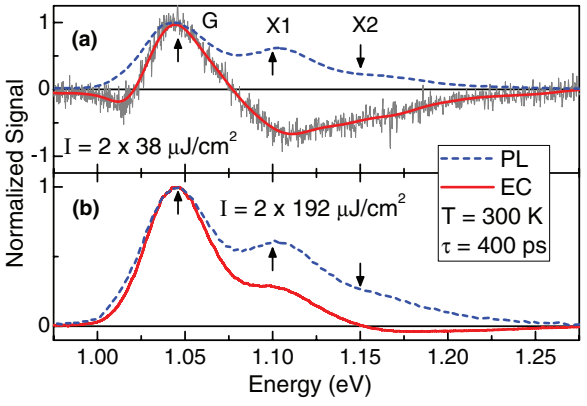


FIG. 3. (Color online) Normalized PL and EC spectra [as defined by Eq. (1)] for (a) $I = 2 \times 38\ \mu J/cm^2$ and (b) $I = 2 \times 192\ \mu J/cm^2$. Note that the sign of the EC signal for the X1 state changes from negative to positive between (a) and (b).

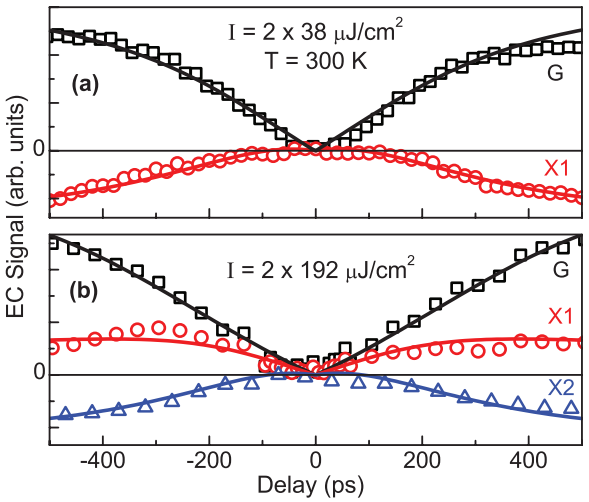


FIG. 4. (Color online) Delay dependence of the EC signal for excitation fluence (a) $I = 2 \times 38\ \mu J/cm^2$ and (b) $I = 2 \times 192\ \mu J/cm^2$ measured at energies indicated by arrows in Fig. 3. The sign of the EC signal from the X1 state is reversed at higher fluence. The solid lines are fits to the data by the model described in the text.

would show up as a decrease in the peak energy due to the temperature-dependent shift in the band gap.

Let us now investigate the time evolution of the EC signal. Figures 4(a) and 4(b) depict, respectively, the EC signal[28] from the G and X1, and G, X1, and X2 states in the delay range of ±500 ps, measured for $I = 2 \times 38$ and $2 \times 192\ \mu J/cm^2$ at the energies marked by arrows on the PL spectra in Fig. 3. It is seen that near zero delay, the signal from the state G is snubbed, while that from the X1 state can be either smaller or larger than the observed signal at longer delay, in agreement with the data in Fig. 3.

Note that the EC measurement is a very sensitive probe of the PL nonlinearity. The EC data in Figs. 3 and 4 detect the PL nonlinearity as a few percent change in the PL intensity, which will not be observable in the steady-state PL data plotted on a log-log scale in Fig. 2 depicting changes over three orders of magnitude. We may also note another difference between the PL data in Fig. 2 and the EC data in Figs. 3 and 4. While Fig. 2 shows the time-integrated (steady-state) PL data, the EC data of Figs. 3 and 4 are both spectrally resolved and time resolved and show how the PL nonlinearity at various energies evolves in time.

A qualitative understanding of the time evolution of the EC data in Fig. 4 is straightforward and the effectiveness of our definition of the EC signal [Eq. (1)] becomes evident at this point. By our definition, the EC signal at a given energy is zero at zero delay ($\tau = 0$). Near zero delay, when both pulses almost simultaneously pump carriers into the QDs, the G state first gets saturated by the carriers at low- and moderate-excitation fluence and excess carriers are pushed to the excited states by virtue of the Pauli exclusion principle. With increasing delay, a fraction of carriers excited by the leading pulse will be lost from the QDs due to radiative and nonradiative recombinations and other carrier loss mechanisms before the second (delayed) pulse pumps more carriers into the QDs. As a result, more carriers from the second pulse can be accommodated in the G state than in the X1 state. Thus the EC signal is positive

(negative) and increases (decreases) with delay for the G (X1) state. At higher-excitation fluence, even the X1 state gets saturated by carriers near $\tau = 0$ and more carriers are pushed to the X2 state. Thus the EC signal is positive for both the G and X1 states and negative for the X2 state. As the delay is increased and carriers are lost from the QDs, the EC signal from the G state continues to increase, the EC signal from the X1 state increases initially and then decreases at long delays, and the EC signal from the X2 state continuously decreases with delay. This is a clear signature of the Pauli blocking in QDs.

To understand these results quantitatively, let us look at the simplest mathematical model that can capture the essential physics of the experiment. Usually these experiments are modeled using rate equations, which, though conceptually simple, have the ugly feature of having a large number of fitting parameters and the solutions are not physically tractable.[10] We shall instead propose a simpler way of looking at the physics by using a thermodynamic argument for the short-time-scale phenomena and a kinetic model for the slower recombination dynamics. The test of the assumptions will lie in the match of the model with observations. Notice that the interband relaxation (radiative and nonradiative recombinations) times lie in the range of a few hundred picoseconds to a few nanoseconds.[9] This is two to three orders of magnitude larger than the intraband relaxation times, which typically are in the range of a few picoseconds at low temperature and would be even shorter at room temperature.[11,13,29] We assume that locally the carriers in a single QD are in thermodynamic equilibrium. In that case, the relative populations of various energy states are simply given by the detailed balance condition

$$\frac{n_j}{n_i} = \frac{g_j}{g_i} \exp\left[ -\frac{\Delta E_{ji}}{k_B T} \right]. \tag{3}$$

Here the labels $i$ and $j$ denote any two excitonic states of a QD, $n_i$ ($g_i$) and $n_j$ ($g_j$) are the corresponding occupation probabilities (degeneracies), $\Delta E_{ji}$ is the energy difference between $i$ and $j$ levels, and $k_B T$ is the thermal energy. The essential nonlinearity in our experiment is associated with the state filling (Pauli blocking) and can be introduced by subtracting the occupation probability from the degeneracy of a given level, i.e., $g_j \to g_j - n_j$. The relative populations should then be rewritten as

$$\frac{n_j(t)}{n_i(t)} = \frac{g_j - n_j(t)}{g_i - n_i(t)} \exp\left[ -\frac{\Delta E_{ji}}{k_B T} \right]. \tag{4}$$

We have made the time dependence of the occupation probabilities explicit here.

It is the time-integrated PL intensity that is measured in the experiment. Hence the PL signal from $i$th excitonic state of an average QD is

$$PL_i = k_i \int_{-\infty}^{\infty} n_i(t) dt, \tag{5}$$

where $k_i$ is the radiative recombination rate of the $i$th state. It is emphasized that since the time scale for the redistribution of the carriers within the QDs is much shorter than the radiative and nonradiative decay times, the net carrier loss rate $\gamma$ ($\geqslant \Sigma_i k_i$), given by the sum of radiative and nonradiative losses through all channels, is all that can be measured in the experiment. Any conventional PL measurement of the time-dependent decay of the individual QD exciton peaks carries little information about the decay rates of individual channels. The only direct way of measuring individual $k_i$ is through the homogeneous linewidth of individual states in single QDs.

In our model we calculate the EC signal numerically. The algorithm for the numerical simulation involves creation of a certain average number of carriers $N(0) \propto I$ within a QD by an excitation pulse of fluence $I$ at time $t = 0$ and distributing them among the QD states according to Eq. (4) to get individual $n_i(0)$. At each time step $t_m$, the total number of carriers $N(t_m) = \Sigma_i n_i(t_m)$ in a QD is reduced by the net loss rate $\gamma$. Assuming monoexponential decay, we write

$$N(t_{m+1}) = N(t_m) - \gamma [t_{m+1} - t_m] N(t_m). \tag{6}$$

While with progressing time carriers are being depleted from the QDs according to Eq. (6), new carriers are added to the QDs at time $t = \tau$ when a second pulse of equal fluence $I$ arrives at the sample. This makes $N(\tau) \to N(\tau) + N(0)$ at $t = \tau$. The distribution of $N(t_{m+1})$ carriers among QD states has been recalculated at each time step using Eq. (4) to get $n_i(t_{m+1})$. This is then used in Eq. (5), which gives time-integrated PL at a given energy at a given delay. This procedure is repeated for several delays and the EC signal is finally calculated using Eq. (1). Notice that if the EC signal at the largest delay ($\tau = \pm 500$ ps) is normalized to one, then for the purpose of fitting the data, the model has only two adjustable parameters: $N$ and $\gamma$.

The solid lines in Figs. 4(a) and 4(b) depict the fits to the data, with $N(0) = 4.5$ and 10.5, respectively, and $\gamma^{-1} = 250$ ps in both cases. The model considered carrier redistribution among six QD states, though the EC signal was calculated for the first two (three) states for the low- (high-) excitation fluence. The level degeneracies[30] were taken as $g_i = 2i$, with $i = 1,2,3,\ldots$ for the G, X1, X2, ... states, respectively. The factor of 2 comes from the spin degeneracy. The thermal energy was taken to be $k_B T = 25$ meV and the energy difference between successive QD states was fixed at $E_{ji} = 50$ meV, as observed for the first three QD states in the experimental PL spectra (Fig. 2). We found that the simulation was insensitive to the addition of more energy levels beyond the sixth QD state. After fitting the model to the normalized EC data, the ratios of the radiative recombination rates $k_i$ for the G, X1, and X2 states are found by rescaling the normalized curves from the model to the actual measured EC intensities for these states. The ratios are expected to depend on the $g_i$'s as well as on the overlap of the initial- and final-state wave functions. The data in Fig. 4(a) for $I = 2 \times 38$ $\mu$J/cm$^2$ were fitted with the ratio $k_1/k_2 \sim 1$, while the data in Fig. 4(b) for $I = 2 \times 192$ $\mu$J/cm$^2$ were fitted with the ratios $k_1/k_2 \sim 2$ and $k_2/k_3 \sim 1$.

The good fit of experimental data using very few parameters and especially the fact that the change in sign of the EC signal with excitation fluence is quantitatively reproduced by this model show that we have been able to capture the essential physics of the EC PL in QDs within our simple model. However, the price of this simplicity is that the average number of carriers $N(0)$ per QD is more of a fit parameter. For example, the values of $N(0)$ that we have obtained, though reasonable, do not scale with the excitation fluence. This is

partly reconciled by the fact that in real Stranski-Krastanow dots there is an additional wetting layer. Beyond some energy above the quantum dot ground state, one no longer has discrete QD states but an extended two-dimensional density of states due to the wetting layer. In the absence of the knowledge of the values of the ground-state energy of the wetting layer, adding this feature to the model is not very meaningful. Even then, we have observed that a much larger value of $N(0)$ is required to fit the high-fluence data [Fig. 4(b)] when the degeneracy of the fourth energy level is arbitrarily increased to qualitatively simulate the effect of wetting layer.

To summarize, we have demonstrated the phenomenon of Pauli blocking in self-assembled InAs/GaAs QDs through the dynamics of the nonlinear PL signal on the picosecond time scale. To do so, we introduced a modification of the EC spectroscopy that gives a physically transparent interpretation of the time-resolved nonlinear PL signal. The experimental results of EC measurements could be quite satisfactorily understood within a simple theoretical model that combined carrier loss kinetics with the principle of detailed balance and the Pauli exclusion principle. An interesting transition from bimolecular recombination at low-excitation fluence to excitonic recombination at higher fluence was also observed.

We thank P. Upadhya for useful discussions related to the experiment. This work was partly supported by DST, India.

*bhavtosh@iiserkol.ac.in
†bipul@iiserkol.ac.in

[1] I. J. Thompson, B. V. Danilin, V. D. Efros, J. S. Vaagen, J. M. Bang, and M. V. Zhukov, Phys. Rev. C **61**, 024318 (2000); C. A. Bertulani and C. De Conti, *ibid.* **81**, 064603 (2010).

[2] B. DeMarco, S. B. Papp, and D. S. Jin, Phys. Rev. Lett. **86**, 5409 (2001); D. J. MacNeill and F. Zhou, *ibid.* **106**, 145301 (2011).

[3] M. Travagnin, Phys. Rev. A **64**, 013818 (2001); I. A. Maione, M. Macucci, G. Iannaccone, G. Basso, B. Pellegrini, M. Lazzarino, L. Sorba, and F. Beltram, Phys. Rev. B **75**, 125327 (2007); J. M. An, A. Franceschetti, and A. Zunger, *ibid.* **76**, 161310 (2007).

[4] R. C. Ashoori, Nature (London) **379**, 413 (1996); U. Banin, Y. Cao, D. Katz, and O. Millo, *ibid.* **400**, 542 (1999).

[5] See, e.g., L. Jacak, P. Hawrylak, and A. Wójs, *Quantum Dots* (Springer, Berlin, 1998); *Self-Assembled InGaAs/GaAs Quantum Dots: Semiconductors and Semimetals*, edited by M. Sugawara (Academic, Toronto, 1999), Vol. 60; Y. Masumoto and T. Takagahara, *Semiconductor Quantum Dots: Physics, Spectroscopy and Applications* (Springer, Berlin, 2002); Z. M. Wang, *Self-Assembled Quantum Dots* (Springer, New York, 2008).

[6] B. T. Miller, W. Hansen, S. Manus, R. J. Luyken, A. Lorke, J. P. Kotthaus, S. Huant, G. Medeiros-Ribeiro, and P. M. Petroff, Phys. Rev. B **56**, 6764 (1997).

[7] M. D. Martín, C. Antón, L. Viña, B. Piętka, and M. Potemski, Europhys. Lett. **100**, 67006 (2012).

[8] S. Raymond, S. Fafard, P. J. Poole, A. Wojs, P. Hawrylak, S. Charbonneau, D. Leonard, R. Leon, P. M. Petroff, and J. L. Merz, Phys. Rev. B **54**, 11548 (1996).

[9] S. Malik, E. C. Le Ru, D. Childs, and R. Murray, Phys. Rev. B **63**, 155313 (2001); A. Melliti, M. A. Maaref, F. Hassen, M. Hjiri, H. Maaref, J. Tignon, and B. Sermage, Solid State Commun. **128**, 213 (2003).

[10] S. Grosse, J. H. H. Sandmann, G. von Plessen, J. Feldmann, H. Lipsanen, M. Sopanen, J. Tulkki, and J. Ahopelto, Phys. Rev. B **55**, 4473 (1997); V. Zwiller, M. E. Pistol, D. Hessman, R. Cederström, W. Seifert, and L. Samuelson, *ibid.* **59**, 5021 (1999).

[11] S. Marcinkevičius and R. Leon, Phys. Rev. B **59**, 4630 (1999); T. Müller, F. F. Schrey, G. Strasser, and K. Unterrainer, Appl. Phys. Lett. **83**, 3572 (2003); G. Rainò, G. Visimberga, A. Salhi, M. De Vittorio, A. Passaseo, R. Cingolani, and M. De Giorgi, *ibid.* **90**, 111907 (2007); H. Kurtze, J. Seebeck, P. Gartner, D. R. Yakovlev, D. Reuter, A. D. Wieck, M. Bayer, and F. Jahnke, Phys. Rev. B **80**, 235319 (2009).

[12] T. Kazimierczuk, M. Goryca, M. Koperski, A. Golnik, J. A. Gaj, M. Nawrocki, P. Wojnar, and P. Kossacki, Phys. Rev. B **81**, 155313 (2010).

[13] T. S. Sosnowski, T. B. Norris, H. Jiang, J. Singh, K. Kamath, and P. Bhattacharya, Phys. Rev. B **57**, R9423 (1998); V. I. Klimov and D. W. McBranch, Phys. Rev. Lett. **80**, 4028 (1998).

[14] L. M. Herz, R. T. Phillips, E. C. Le Ru, and R. Murray, Phys. Status Solidi A **190**, 565 (2002).

[15] J. Urayama, T. B. Norris, H. Jiang, J. Singh, and P. Bhattacharya, Appl. Phys. Lett. **80**, 2162 (2002).

[16] V. Esch, B. Fluegel, G. Khitrova, H. M. Gibbs, X. Jiajin, K. Kang, S. W. Koch, L. C. Liu, S. H. Risbud, and N. Peyghambarian, Phys. Rev. B **42**, 7450 (1990).

[17] R. J. Warburton, C. S. Dürr, K. Karrai, J. P. Kotthaus, G. Medeiros-Ribeiro, and P. M. Petroff, Phys. Rev. Lett. **79**, 5282 (1997); M. Jung, K. Hirakawa, Y. Kawaguchi, S. Komiyama, S. Ishida, and Y. Arakawa, Appl. Phys. Lett. **86**, 033106 (2005).

[18] U. Bockelmann and T. Egeler, Phys. Rev. B **46**, 15574 (1992); P. Borri, S. Schneider, W. Langbein, and D. Bimberg, J. Opt. A: Pure Appl. Opt. **8**, S33 (2006); K. Hyeon-Deuk and O. V. Prezhdo, J. Phys.: Condens. Matter **24**, 363201 (2012).

[19] M. B. Johnson, T. C. McGill, and A. T. Hunter, J. Appl. Phys. **63**, 2077 (1988); J. L. A. Chilla, O. Buccafusca, and J. J. Rocca, Phys. Rev. B **48**, 14347 (1993).

[20] D. von der Linde, J. Kuhl, and E. Rosengart, J. Lumin. **24/25**, 675 (1981); D. Rosen, A. G. Doukas, Y. Budansky, A. Katz, and R. R. Alfano, Appl. Phys. Lett. **39**, 935 (1981); B. Pal, A. V. Gopal, S. S. Prabhu, and A. S. Vengurlekar, Phys. Rev. B **65**, 045312 (2002); H. Hirori, K. Matsuda, Y. Miyauchi, S. Maruyama, and Y. Kanemitsu, Phys. Rev. Lett. **97**, 257401 (2006); Horng-Chang Liu, Chia-He Hsu, Wu-Ching Chou, Wei-Kuo Chen, and Wen-Hao Chang, Phys. Rev. B **80**, 193203 (2009).

[21] J. Shah, *Ultrafast Spectroscopy of Semiconductors and Semiconductor Nanostructures* (Springer, Berlin, 1999).

[22] M. D. Sturge, Phys. Rev. **127**, 768 (1962).

[23] H. R. Phillip and H. Ehrenreich, Phys. Rev. **129**, 1550 (1963).

[24] W. Pickin and J. P. R. David, Appl. Phys. Lett. **56**, 268 (1990).

[25] K. Brunner, G. Abstreiter, G. Böhm, G. Tränkle, and G. Weimann, Phys. Rev. Lett. **73**, 1138 (1994); S. Amloy, E. S. Moskalenko, M. Eriksson, K. F. Karlsson, Y. T. Chen, K. H. Chen, H. C. Hsu, C. L. Hsiao, L. C. Chen, and P. O. Holtz, Appl. Phys. Lett. **101**, 061910 (2012).

[26] Y. Masumoto, S. Yoshida, M. Ikezawa, S. Tomimoto, and Y. Sakuma, Appl. Phys. Lett. **98**, 061905 (2011).

[27] Y. Masumoto, S. Tarucha, and H. Okamoto, J. Phys. Soc. Jpn. **55**, 57 (1986); B. Pal and A. S. Vengurlekar, Phys. Rev. B **66**, 155337 (2002).

[28] While care was taken to make the intensities of the two pulses the same, a slight difference in the intensities was observed as the delay stage moved from one end to the other, possibly due to a small divergence of the laser beam. This led to a small linear background, which gave an overall tilt to the EC signals. This linear background (calculated using an unbiased computer program) was subtracted from the experimental EC signal in Fig. 4.

[29] B. Pal and A. S. Vengurlekar, Appl. Phys. Lett. **79**, 72 (2001).

[30] S. Awirothananon, S. Raymond, S. Studenikin, M. Vachon, W. Render, A. Sachrajda, X. Wu, A. Babinski, M. Potemski, S. Fafard, S. J. Cheng, M. Korkusinski, and P. Hawrylak, Phys. Rev. B **78**, 235313 (2008).